Localized MRS Employing Radiofrequency Field (B_1) Gradients

Michael Garwood

University of Minnesota, Minneapolis, MN, USA

This article describes techniques that have been developed to localize MRS (magnetic resonance spectroscopy) spectra using the spatially dependent magnetic field (B_1) produced by one or more RF coils. The work is focused on the two main techniques previously shown to be capable of producing high-quality localized spectra, which are (i) depth pulse sequences and (ii) rotating frame zeugmatography and its variant, the Fourier series window method. As compared with the now more commonly used localization techniques that exploit spatial gradients in the main field (B_0), these B_1-gradient techniques still offer advantages, including (i) avoidance of spectral distortions due to eddy currents, (ii) elimination of acoustic noise, and (iii) minimization of signal loss due to the rapid decay of the transverse magnetization. The drawbacks of B_1-gradient methods, such as their limited flexibility to define the voxel shape, are discussed together with some ways to overcome their shortcomings. A description of the experimental procedures required to implement B_1-gradient methods is also included.

Keywords: NMR, MRS, localized spectroscopy, surface coil, depth pulse, rotating frame zeugmatography, Fourier series window, in vivo ^{31}P MRS

How to cite this article:
eMagRes, 2016, Vol 5: 1015–1026. DOI 10.1002/9780470034590.emrstm1440

Introduction

Tremendous excitement was sparked in biochemistry and physiology laboratories around the world following publication of the first in vivo surface coil magnetic resonance spectroscopy (MRS) study of organ metabolism.[1] With its simple planar loop geometry, the surface coil provided a convenient new probe for in vivo MRS experimentation, and it provided unmatched high sensitivity localized to a roughly hemispherical volume adjacent to the coil.

The greatest magnetic flux of the RF field (B_1) by a surface coil occurs inside the plane circumscribed by the coil loop(s). Away from this plane, B_1 drops off in both radial and axial (depth) directions. As such, when using a surface coil to excite spins with a conventional hard (or square) RF pulse, the flip angle (θ) varies spatially, and when using such coil for signal detection, its sensitivity drops off in both radial and axial directions. Early in vivo MRS studies exploited this positional dependence of the surface coil B_1 to achieve a rudimentary degree of spatial localization.

With a surface coil, the pulse duration (t_p) can be adjusted to produce a near optimal flip angle (i.e., the Ernst angle-see ***The Basics***) at a depth corresponding roughly to the organ or tissue of interest, while larger flip angles ($\theta \approx 180^\circ$) occur in tissues closer to the surface and thus unwanted intervening signal can be partially suppressed. Although this simple approach provides sufficient localization for some types of anatomy, greater precision in defining the volume of interest (VOI) is required for most applications of MRS. In locations adjacent to the coil loop, the B_1 gradient is very steep and thus rapid spatial variation of the flip angle θ occurs in these 'high-flux regions'. When performing MRS measurements on deep tissue regions, it is difficult to avoid flip angles that leave the magnetization (**M**) fully excited in the transverse plane (e.g., $\theta = 270^\circ$ and 450°) in these shallow regions. Because these high-flux regions also correspond to the regions of highest coil sensitivity during signal reception, a large amount of signal contamination inevitably arises close to the coil.

Thus, in the early days of surface coil MRS circa 1981–1985, much effort was devoted to developing techniques that would provide improved control in positioning the VOI and that could achieve precise localization. To attain greater localization precision, some early promising techniques combined the use of surface coils with pulsed gradients in the main magnetic field, B_0, used in MRI.[2,3] However, these works occurred before actively shielded B_0 gradients were introduced, and some researchers at the time, including this author, believed the use of B_0 gradients to be incompatible with MRS, as on/off switching of B_0-gradient coils in those days gave rise to large eddy currents that decayed slowly (for tens to hundreds of milliseconds) during FID acquisition and these eddy currents severely degraded spectral quality. As a result, spatial localization techniques that used only the B_1 gradients produced by surface coils were born. These are the topics of this article.

Still today, avoiding the use of pulsed B_0 gradients can be advantageous beyond circumventing problems caused by eddy currents. For example, B_1 gradients can be switched on and off rapidly in 1–2 μs, and unlike B_0-gradient coils, negligible eddy currents and acoustic noise are produced when pulsing B_1 coils. Furthermore, unlike many of the contemporary B_0-gradient techniques, B_1-localization techniques can be performed without spin- or stimulated-echo acquisitions, which inevitably forfeit signals from many low-gyromagnetic ratio (γ) nuclei that have spin–spin relaxation time (T_2) values comparable to or less than the minimum achievable echo time, TE. Finally, owing to recent developments in parallel transmit capabilities with multicoil arrays, which can irradiate RF simultaneously and independently, the prospects for achieving much greater localization precision and the potential for new effective B_1-gradient techniques have led to exciting possibilities in this area. To date, these new methods have been applied in MRI only. Therefore, the focus of this article will be restricted to the classical B_1-localization techniques that have previously yielded meaningful biomedical data in multinuclear MRS studies of organs.

The techniques to be described herein use various RF pulsing schemes to achieve localization by exploiting the spatially dependent B_1 of one or more surface coils. These techniques fall into three main categories with the following designations: (i) composite pulse localization, (ii) depth pulse sequences, and (iii) rotating frame zeugmatography (RFZ). All of these methods have their limitations. In practice, the most significant among them is their limited ability to control the shape and positioning of the localized volume. Specifically, it is difficult to sculpt the shape and dimensions of the VOI and to position the VOI off axis from the coil. Matching the VOI shape and size to the anatomy of interest is often essential to achieve a sufficient signal-to-noise ratio (SNR) for successful MRS. Fortunately, this limitation can be partially mitigated using multiple coils. Another challenge is maintaining a fixed position and high spatial selectivity of the volume when the spectra have broad chemical shift dispersion, as in the case of ^{13}C and ^{31}P MRS. Specifically, with conventional hard pulses, the RF pulse frequency coincides with the Larmor frequency at one spectral position only (i.e., corresponding to the 'on-resonant' isochromat at the carrier frequency). Off-resonance excitation of the other spectral components unfavorably affects their spatial localization when using any of the existing B_1-localization methods. These problems and ways to minimize them will be discussed herein.

A composite pulse is a sequence of phase-shifted hard pulses applied without delays between pulses. In composite pulse localization methods, the pulses have a prescribed set of durations and phases designed to produce a particular spin manipulation or flip angle in a selected region of interest only. Most composite pulse localization strategies require subtracting FIDs produced by sequences applying different transmitter and receiver phases, or by switching certain pulses on and off. Two types of composite pulse techniques were originally introduced and both are based on using special composite pulses designed to produce a flip angle of 180° only in the VOI. In the NOBLE (narrow-band localized excitation) method by Tycko and Pines,[4] two acquisitions are performed, one with and another without a composite 180° pulse preceding the excitation pulse. This 180° 'prepulse' produces a spatially selective inversion of the initial magnetization. After subtracting FIDs acquired with and without this prepulse, signal in the VOI adds constructively, while signals outside the VOI are negated. In the composite pulse method of Shaka and Freeman,[5–7] the composite 180° pulse follows the excitation pulse and subtraction is accomplished by phase cycling the composite pulse. This phase-cycling scheme, which is called *EXORCYCLE* (a 4-step phase cycle for spin echoes),[8] is a fundamental element of other localization methods, particularly depth pulse sequences, and it will be described in greater detail later.

In the original depth pulse method,[9] composite 180° pulses are not used. Instead, combinations of the signal elimination schemes described above are used with simple hard pulses. Specifically, a set of FIDs is acquired using prescribed on/off settings of prepulses and alterations of transmitter and receiver phases. As compared with composite pulse methods, depth pulse sequences generally attain a similar precision of localization using a smaller minimum number of FID acquisitions. In addition, the off-resonance performance of depth pulses is generally better than that of composite pulse methods. For these reasons, the depth pulse method was preferred over composite pulses for single-voxel localization in the early days of in vivo MRS.

RFZ was the first B_1-localization method to be introduced.[10] RFZ's ability to perform multivoxel localization is one of its main advantages over the other B_1-localization methods. In RFZ, a set of FIDs is acquired using an excitation pulse that incrementally increases in duration, t_p. By exciting FIDs with incrementally increased t_p, spatial information is encoded in the nutation frequency of the magnetization. The type of spatial encoding (amplitude versus phase modulation) contained in the consecutively acquired FIDs depends on the choice of sequence used, as discussed later. Finally, an abbreviated version of the RFZ method called *Fourier series windows* (*FSW*) permits single-voxel MRS with similar performance as in depth pulse. In addition, acquisition-weighted FSW provides a means to maximize SNR for multivoxel MRS and therefore will be briefly described.

The majority of MRS studies utilizing B_1 gradients for spatial localization have utilized depth pulse and RFZ methods. Therefore, this article focuses mainly on the principles and experimental implementations of these two techniques.

Basics

At any given position in an object of interest, the signal intensity produced by a hard pulse applied on resonance is proportional to $B_1^-(\mathbf{r})\sin\theta(\mathbf{r})$, where the vector $\mathbf{r}$ expresses the positional dependencies of the flip angle (θ) and the receptive field amplitude (B_1^-) returned by the coil(s) used for signal detection. In the descriptions that follow, the signal's dependence on B_1^- will be neglected and only the spatial selectivity provided by the different transmitted field (B_1^+) will be considered, as done in the original articles on depth pulse methods. In addition, for brevity, the dependency of θ on $\mathbf{r}$ will be implicit.

An important feature of any MRS localization method is how well it tolerates a resonance offset, $\Delta\nu$, due to chemical shift. In a frame of reference rotating at the NMR frequency, denoted (x', y', z'), the axis of off-resonance rotation is tilted out of the transverse ($x'y'$) plane by the angle

$$\alpha = \frac{\Delta \nu}{4t_{90}} \quad (1)$$

where t_{90} is the pulse duration needed to produce a 90° flip angle at a given location in the object. In this frame, the off-resonance effective field amplitude is

$$B_{\mathrm{eff}} = B_1^+ \sec \alpha \quad (2)$$

Accordingly, the off-resonance rotation produced by B_{eff} is larger than the on-resonance rotation, as given by

$$\theta' = \theta \sec \alpha \quad (3)$$

Off-resonance effects are responsible for signal attenuation and displacement of the B_1-localized volume, as will be shown.

The spin-echo sequence element, 90°-τ-180°-τ-, is used ubiquitously in high-resolution NMR spectroscopy, MRI, and other applications of NMR. When performing spin-echo spectroscopy, an imperfect refocusing pulse can cause phase distortion and spectral artifacts. In such cases, the four-step EXORCYCLE phase cycle, written [$\pm x$, $\pm y$], has been used to eliminate these effects.[8] This phase cycle subtracts the signal components that evolve on any coherence pathway that does not lead to a spin echo. To properly combine the signals of this four-step sequence, the phase of the receiver must be inverted when the phase of the refocusing pulse is either $+y$ or $-y$.

The Depth Pulse Method

Depth Pulse Principles and Sequences

The depth pulse method was first described by Bendall and Gordon in 1983.[9] They suggested applying some pulses of a depth pulse sequence with one coil and other pulses with a second coil as a means to sculpt the voxel, although this was technically challenging at the time. Nowadays, such multicoil transmit systems are becoming more available, and although still under development, advanced multicoil approaches for localizing are expected to offer large improvements and new capabilities for in vivo MRS in the future. However, for the sake of simplicity, the current descriptions will be confined to experimental implementations using one coil or two coplanar concentrically arranged surface coils. With this simplified approach, the VOI must always be positioned symmetrically on the axis of the coil(s), and its shape and depth are dictated by the specifics of the coil geometries used, the choice of pulse sequence, and the RF amplitudes (or pulse durations). The need to restrict the localized region to an axial position is one major drawback to this type of B_1-localization approach and requires that MRI be used to guide the placement of the coil(s) directly over the tissue of interest.

As noted above, EXORCYCLE is a fundamental element in depth pulse sequences. The most basic depth pulse sequence is simply a spin-echo sequence using EXORCYCLE and can be written as

$$\theta - \tau - 2\theta[\pm x, \pm y]\text{-}\tau\text{-acquire} \quad \text{(A)}$$

This nomenclature describes a sequence of two consecutive hard pulses (θ and 2θ) separated by an optional delay, τ.

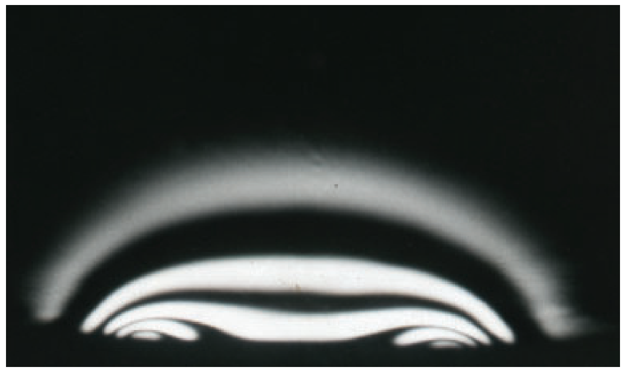

Figure 1. Image of the signal intensity excited and detected by a surface coil using sequence (A). The image intensity is a function of the flip-angle variation in a transverse (xy) plane bisecting the center of the coil ($z = 0$)

In most applications of the depth pulse method, τ can be set to zero, although a $\tau > 0$ is useful when the goal is to measure T_2 or perform ^{13}C polarization transfer experiments. The use of θ to denote a pulse emphasizes the fact that the flip angle produced by the pulse varies continuously in the object when transmitting with a surface coil. In addition, by this nomenclature, 2θ indicates a pulse that is twofold longer than the θ pulse, and accordingly, the flip angle at every location is twice that produced by the θ pulse. Square brackets contain the set of RF phases through which a pulse must be cycled. A lack of phases in brackets after a pulse (e.g., the θ pulse in this sequence) means that the phase of that pulse is inconsequential and its value remains constant in repetitions of the sequence.

The 2θ-refocusing pulse using EXORCYCLE imparts signal dependence proportional to $\cos^2\alpha \sin^2\theta'$.[11] Thus, with sequence (A) the on-resonance signal is proportional to $\sin^3\theta$. The image in Figure 1 shows the spatial dependence of the signals excited on-resonance with sequence (A) using a single surface coil for RF transmission and reception. It can be seen that signal arises only in regions where θ is close to an odd multiple of 90°, in agreement with the theoretically predicted $\sin^3\theta$ dependence. This result also illustrates the inability to obtain a fully localized VOI when using a single surface coil to perform the measurement. Specifically, the $\theta = 90°$ region unavoidably intersects the object's surface and unwanted signals are excited in high-flux regions where the flip angle approximates 270°, 450°, 630°, etc.

In their original work, Bendall and Gordon described the phase-cycled depth pulse sequence

$$2\theta;\ \theta[\pm x];\ (2\theta[\pm x, \pm y])_2;\ \text{acquire} \quad \text{(B)}$$

This sequence consists of four consecutive pulses producing flip angles: 2θ, θ, 2θ, and 2θ, respectively. Note that the subscripted 2 after the parentheses around $2\theta[\pm x, \pm y]$ indicates two repetitions of this element. Sequence (B) contains another type of 2θ element, which functions as an inversion pulse before the excitation pulse. In this sequence, the phase of the receiver is cycled together with the phase of the excitation pulse, $\theta[\pm x]$. With sequence (B), a total of 32 FIDs (or transients) are needed to complete the phase cycle and achieve the desired spatial selectivity. Table 1 shows the set of phases of the pulses

Table 1. Relative pulse and receiver phases of depth pulse sequence (B): 2θ; $\theta[\pm x]$; $(2\theta[\pm x,\pm y])_2$; acquire

Transient #	2θ	θ	2θ	2θ	acq
1	x	x	x	x	x
2	x	$-x$	x	x	$-x$
3	x	x	y	x	$-x$
4	x	$-x$	y	x	x
5	x	x	$-x$	x	x
6	x	$-x$	$-x$	x	$-x$
7	x	x	$-y$	x	$-x$
8	x	$-x$	$-y$	x	x
9	x	x	x	y	$-x$
10	x	$-x$	x	y	x
11	x	x	y	y	x
12	x	$-x$	y	y	$-x$
13	x	x	$-x$	y	$-x$
14	x	$-x$	$-x$	y	x
15	x	x	$-y$	y	x
16	x	$-x$	$-y$	y	$-x$
17	x	x	x	$-x$	x
18	x	$-x$	x	$-x$	$-x$
19	x	x	y	$-x$	$-x$
20	x	$-x$	y	$-x$	x
21	x	x	$-x$	$-x$	x
22	x	$-x$	$-x$	$-x$	$-x$
23	x	x	$-y$	$-x$	$-x$
24	x	$-x$	$-y$	$-x$	x
25	x	x	x	$-y$	$-x$
26	x	$-x$	x	$-y$	x
27	x	x	y	$-y$	x
28	x	$-x$	y	$-y$	$-x$
29	x	x	$-x$	$-y$	$-x$
30	x	$-x$	$-x$	$-y$	x
31	x	x	$-y$	$-y$	x
32	x	$-x$	$-y$	$-y$	$-x$

and receiver, as used in this sequence. To achieve sufficient SNR, MRS measurements usually require signal averaging, and therefore, the need to acquire a minimum of 32 transients or even multiples of 32 transients (i.e., 64, 96, 128, ...) typically is not a drawback. On resonance, sequence (B) yields a signal proportional to $-\cos(2\theta)\sin^5\theta$, and therefore, the widths of the excited bands are narrower than those obtained with sequence (A) shown in Figure 1.

In later work,[12] sequence (B) was shown to be equivalent to

$$2\theta[\pm x];\, \theta;\; (2\theta[\pm x, \pm y])_2;\; \text{acquire} \qquad \text{(C)}$$

As compared with sequence (B), the complexity of phase cycling is reduced with sequence (C) because the receiver phase is inverted only when applying a $2\theta[\pm y]$ pulse. When collecting transients produced with two $2\theta[\pm y]$ pulses, the receiver phase is not inverted. Another useful feature of sequence (C) is that T_1 can be measured by inserting a variable delay between the $2\theta[\pm x]$ prepulse and the θ excitation pulse.

As time progressed, Bendall and coworkers introduced more complex depth pulse sequences to further reduce the size of the VOI and, more importantly, avoid signals from high-flux regions. One sequence element for improving localization is written as $2\theta[\pm x, \bar{0}]$, which means two transients are produced with a 2θ pulse having phases $+x$ and $-x$, and then two transients are collected without application of this pulse, but with an inverted receiver phase.[11]

In addition to the $2\theta[\pm x]$ prepulses, $4\theta[\pm x]$, $6\theta[\pm x]$, and $8\theta[\pm x]$ prepulses were also shown to have utility.[11] In separate work, Shaka and Freeman[6,13] introduced the useful sequence element written in depth pulse nomenclature as $4\theta\left[\pm x\left(\frac{2}{3}\right), 0\left(\frac{1}{3}\right)\right]$, whereby the 4θ prepulse is applied for 2/3 of the transients and not applied for 1/3 of the transients, with no inversion of the receiver phase.

Another approach used to improve the degree of localization involves adding (or subtracting) transients produced with excitation pulses of different flip angles, such as θ, 3θ, and 5θ ....[11] One sequence using this approach is

$$2\theta[\pm x];\; \{\theta - 3\theta\};\; 2\theta[\pm x, \pm y];\; \text{acquire} \qquad \text{(D)}$$

In sequence (D), the negative sign in front of the 3θ pulse implies FID subtraction or, equivalently, receiver phase inversion when acquiring this transient.[14] A sequence of this type that yields an even smaller VOI is

$$2\theta[\pm x];\; 4\theta[\pm x];\; \{\theta - 3\theta + 5\theta - 7\theta + 9\theta\};$$
$$2\theta[\pm x, \pm y];\; \text{acquire} \qquad \text{(E)}$$

Note that the length of sequence (E) can be a practical drawback, particularly when the RF power deposition exceeds safe limits and/or the relaxation time is similar to the total sequence duration, as this leads to SNR loss.

A final type of prepulse element is used to eliminate high-flux signals. These have the form, $\theta/3[\pm x]$, $\theta/5[\pm x]$, $2\theta/3[\pm x]$, and $4\theta/3[\pm x]$.[11,12] When eliminating high-flux signal in this manner (i.e., using prepulses of flip angle different from 2θ), the VOI signal is diminished. Accordingly, the use of such elements is undesirable, yet unavoidable in many cases. In general, these types of prepulses are necessary whenever the desired VOI depth exceeds the physical dimension of the coil radius.

Limitations of Depth Pulse Sequences

As mentioned above, the VOI shape, location, and SNR have complex dependencies on chemical shift (or offset frequency, $\Delta\nu$). Different methods and sequences offer varying degrees of sensitivity to resonance offset, and this should be considered when choosing an MRS sequence for any given application. Contour plots showing the calculated signal intensity produced by sequences (D) and (E) as a function of flip angle and resonance offset are shown in Figure 2. In the plots, the offset axis (vertical) is defined in terms of the pulse duration (t_{90} or t_θ) needed to produce a flip angle (90° or θ, respectively). The absolute offset (in Hz) is obtained by dividing the value of the offset scale by the value of t_{90} or t_θ used. In these examples, a scaled offset of 0.1 corresponds to an approximate 50% loss of signal intensity. For example, assuming $t_{90} = 100$ μs in the VOI, a spectral peak that resonates at $\Delta\nu = 1000$ Hz suffers ~50% signal reduction relative to the spectral peak at $\Delta\nu = 0$. Increasing loss of signal as a function of the absolute value of the resonance offset, $|\Delta\nu|$, is due to the limited bandwidth of the pulses. In general, as the depth pulse sequence

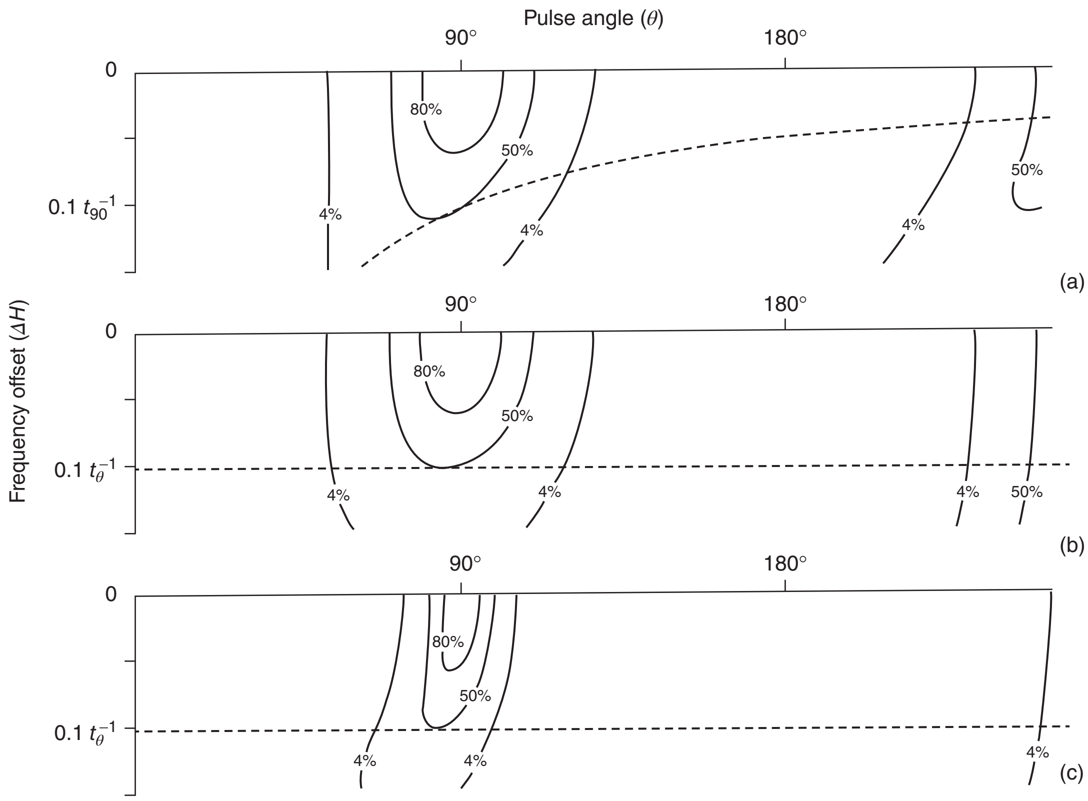

Figure 2. Contour plots showing the calculated signal intensity produced by sequences (D) and (E), as a function of flip angle and resonance offset. The offset axis (vertical) is defined in terms of the pulse duration (t_{90} and t_θ, respectively) needed to produce (a) a flip angle $\theta = 90°$ or (b,c) an arbitrary flip angle θ. The actual offset (in Hz) is obtained by dividing the value of the offset scale by the value of t_{90} or t_θ. The dashed line indicates where 50% signal loss occurs. (Reproduced from Ref. 14. © Elsevier, 1969)

gets longer, the loss of signal intensity occurs more rapidly as $|\Delta\nu|$ increases. This problem can limit the use of longer depth pulse sequences, particularly for human applications where the available transmit field (B_1^+) with larger surface coils constrains the minimum achievable t_{90} to much larger values (e.g., 250–750 μs).

Multicoil Implementations of Depth Pulse

An exemplary demonstration of the high quality of ^{31}P spectra obtainable with depth pulse sequences in animals can be seen in Figure 3. Shown are the first in vivo spectra ever obtained from a completely isolated volume using only B_1 gradients.[15] In this work, unwanted signal from high-flux regions was avoided using two concentric coils having different diameters. Some pulses in the depth pulse sequence were transmitted using the large coil while others were transmitted using the small coil, and then the signal was detected with the small coil. ^{31}P contour plots derived from images of the sensitive volumes produced with these two surface coils are shown in Figure 4. It can be seen that the shape, and in particular the transaxial width of the localized volume, does not provide suitable localization when transmitting all pulses through the large coil and using the small coil only for reception (Figure 4a). However, the double transmit method substantially improves the delineation of the sensitive volume by reducing its radial dimensions and sharpening its edges all around (Figure 4b).

Rotating Frame Zeugmatography

RFZ Principles

The RFZ method was introduced before the advent of surface coils. The method was originally proposed as a spatial-encoding strategy for MRI that used B_1 gradients instead of the usual B_0 gradients. In the original MRI experiments described in the classic paper by Hoult,[10] spatial encoding in one direction was achieved with the B_1 gradient of a modified Helmholtz coil, whereas a pulsed B_0 gradient was applied during acquisition to obtain spatial encoding in a second dimension. A year later, Cox and Styles eliminated the B_0 gradient and instead acquired the spectroscopic information in the FIDs.[16] They demonstrated the first one-dimensional (spatial) RFZ spectroscopic localization using two tubes filled with different deuterium compounds. In that work, the B_1 gradient was produced with an asymmetric transmitter coil wound with three turns and one opposed, while an orthogonal 2-turn cylindrical coil was used for reception.[16] Approximately 3 years later, Haase *et al.*[17] performed the first demonstration of one-dimensional surface coil RFZ using three bulbs containing mixtures of phosphates that were stacked on the coil axis. Soon to follow were the first demonstrations of one-dimensional localization of ^{31}P metabolites in intact tissue,[18] and 1 year later, in a human.[19]

Like other Fourier imaging methods, RFZ encodes spatial information from all spatial coordinates simultaneously. RFZ

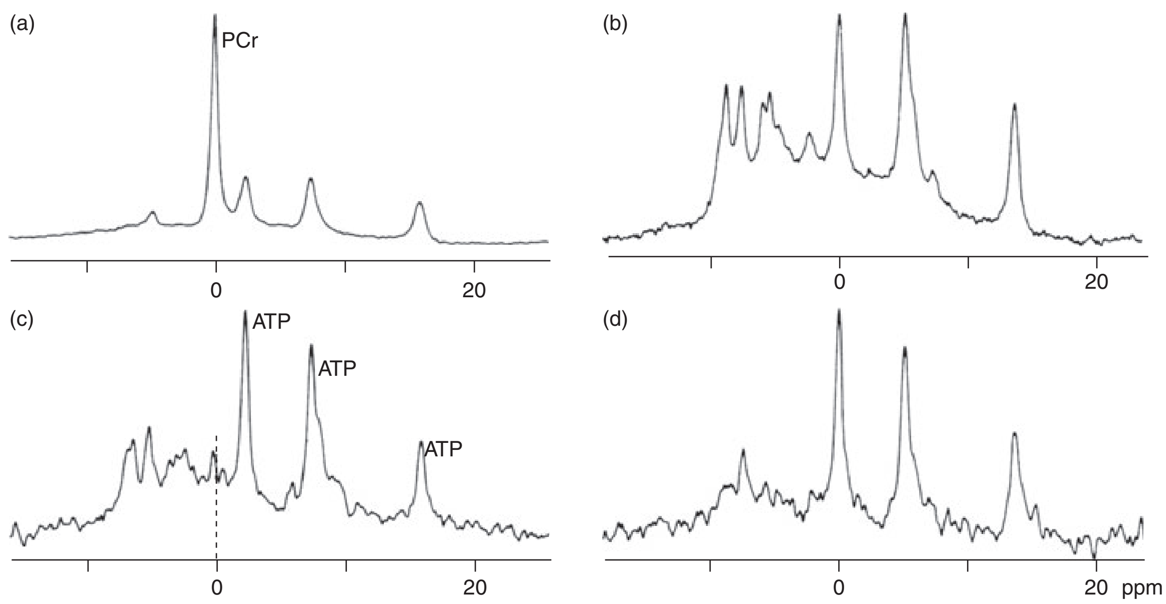

Figure 3. ^{31}P spectra from an anesthetized rat. The spectra shown are from (a) leg muscle, (b) exposed liver, and (c,d) liver in an intact rat. The fully localized spectra (c,d) were obtained using only the B_1 gradients produced by two surface coils. The depth pulse sequence used for (c) and (d) was $2\phi[\pm x, \bar{0}]$; $(\theta/3[\pm x])_2$; $2\theta[\pm x]$; $4\theta\left[\pm x\left(\frac{2}{3}\right), 0\left(\frac{1}{3}\right)\right]$; θ; $2\theta[\pm x, \pm y]$; acquire(Φ), where θ and ϕ represent pulses transmitted via the large (Θ) and small coils (Φ), respectively. A noticeable reduction (30%) in signal intensity from the β-phosphate of adenosine triphosphate (ATP) is a consequence of its resonance offset (PCr = phosphocreatine). (Reproduced from Ref. 15. © Elsevier, 1969)

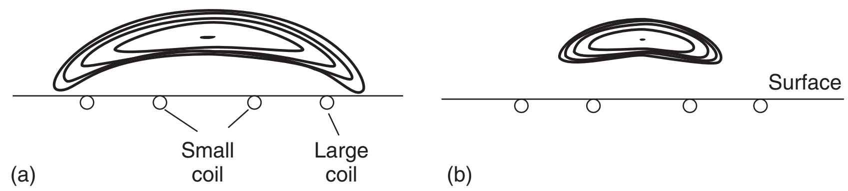

Figure 4. Experimental contour plots derived from ^{31}P images of a phantom depicting the sensitive volume produced by two concentric surface coils. The diameters of the large and small coils were 4.5 and 1.7 cm, respectively, and are drawn to scale in the figures. The contour plots show the image intensities obtained when the depth pulse sequence is transmitted with (a) the large coil only or (b) both coils. In each case, the signal was detected using the small coil only. The double transmit method (b) yields a well-demarcated sensitive volume. (Reproduced from Ref. 15. © Elsevier, 1969)

utilizes FT of amplitude- or phase-modulated time-domain signals to obtain a spectroscopic image. Except for the fact that B_1 gradients are utilized instead of B_0 gradients, RFZ has much in common with conventional Fourier-encoded MRI techniques.

The phase-modulated RFZ sequence can be written as

$$n\theta[x];\ 90^\circ[\pm y];\ \text{acquire} \qquad \text{(F)}$$

where n is an integer representing the pulse increment number. The three elements of this sequence involve (i) transmitting the $n\theta[x]$ pulse using a B_1-gradient coil that rotates $\mathbf{M}$ to a spatially dependent flip angle in the $y'z'$-plane, (ii) applying a 90° pulse along the $+y'$ (or $-y'$) axis to rotate $\mathbf{M}$ to the $x'y'$-plane, and (iii) FID acquisition. This sequence is repeated with n ranging from 1 to N. The incremented pulse duration (nt_p) gives rise to a spatially varying phase modulation, $n\theta(\mathbf{r})$, in the object. Two-dimensional (2-D) FT of the FIDs yields chemical shift spectra as a function of the excitation field $B_1^{\,+}(\mathbf{r})$.

Data processing in RFZ usually consists of the following steps: (i) Starting with the time-domain data acquired using the $90^\circ[+y]$ pulse, FT of the acquired FIDs produces a set of spectra representing the N different pulse durations used. (ii) The phase of the first ($n = 1$) spectrum is adjusted to achieve absorptive (Lorentzian) line shapes in the spectrum. (iii) The resulting spectral phase setting is then applied to all N spectra. (iv) An FT is then performed in the second (nt_p) dimension to obtain a set of spectra as a function of $B_1^{\,+}(\mathbf{r})$. (v) Steps 1, 3, and 4 are repeated on the data acquired with the $90^\circ[-y]$ pulse, using the same spectral phase setting. (vi) These two separately processed data sets are then subtracted to eliminate dispersive components in the final spectra.

For maximum SNR, the $90^\circ[\pm y]$ rotation should be spatially uniform throughout the object. This element of the sequence can be performed using either a frequency-modulated pulse that can perform a 90° plane rotation with an inhomogeneous B_1 (e.g., a B_1-insensitive rotation, BIR-4, adiabatic pulse[20]) or by transmitting a square pulse via a separate coil that can provide a homogeneous B_1 across the VOI. Alternatively, at the expense of a $\sqrt{2}$ reduction in SNR, the 90°[±y] pulse can be simply omitted, in which case the signal is amplitude modulated and the subtraction step described above is not performed.

To maximize SNR, an optimum sequence repetition period (TR) should generally be used (i.e., TR ∼1.2 times T_1, the spin–lattice relaxation time), in which case the magnetization will be partially saturated. In phase-modulated RFZ, the 90°[±y] pulse ensures that immediately after applying the pulses, **M** lies in the transverse plane and thus the recovery of the longitudinal magnetization during every TR period remains unchanged when stepping through the different $n\theta$ values. On the other hand, whenever TR is less than $\sim 3T_1$ in amplitude-modulated RFZ, the level of saturation changes as $n\theta$ is stepped, which leads to spatial blurring.[18] Some methods have been developed to overcome this problem, including using an additional RF pulse after each FID is acquired to null the longitudinal magnetization before beginning each recovery period.[18] The latter approach comes with the disadvantages of reducing the efficiency of data collection and increasing the RF power deposition. Alternatively, a longitudinally modulated version of RFZ overcomes the spatial blurring problem without these drawbacks.[21,22]

Hoult[10] provided the theory describing the achievable spatial resolution of RFZ. He showed that to resolve signals from two locations, a flip angle difference of 270° or greater must exist between them after the Nth pulse increment. Equivalently, the number of resolvable regions in the direction of the B_1 gradient can be no larger than $2N/3$. The latter theoretical description assumes no relaxation during the pulse(s), which for some fast relaxing nuclei is not justified and will thus need to be accounted for. To achieve adequate SNR within the allowable scan time, N might need to be restricted to a relatively small number (e.g., $N \sim 8$–16), and as a result, truncation artifacts might appear in the spatial dimension. In this case, multiplication by a function that decays as nt_p increases (i.e., an exponentially decaying function) may be used to minimize such truncation artifacts (also known as *Gibbs wobbles* or *ringing*), albeit at the expense of spatial resolution. An alternative approach that can significantly improve SNR over this standard apodization procedure is to set the number of transients acquired at each setting of n proportional to the corresponding Fourier coefficient as described below.

The FSW Modification

As an alternative to the multiregion encoding of RFZ, a single region of interest can be localized with the amplitude-modulated RFZ using a Fourier series formalism. With this FSW approach,[23–26] SNR of the amplitude-modulated RFZ can be improved by setting the number of transients averaged at each setting of the pulse duration (nt_p), to be proportional to the Fourier coefficient of the nth discrete point in this domain. For example, to achieve localization in a spatial region centered at $\theta(\mathbf{r}) = 90°$, nonzero coefficients exist only for odd multiples of n, and thus, transients corresponding to even multiples of n need not be acquired. The first 5 nonzero coefficients are approximately proportional to 9, 8, 6, 3, and 1. Thus, SNR is maximized and Gibbs wobbles are minimized when the flip angle in the VOI is stepped through 90°, 270°, 450°, 630°, and 810° and the number of transients averaged at each is a multiple of 9, 8, 6, 3, and 1, respectively. FIDs acquired with these prescribed flip-angle settings are added or subtracted in accordance with their Fourier series coefficients. With the FSW approach, the width of the resulting localized region (expressed in terms of $\Delta\theta$) is approximately the same as that achieved with most depth pulse sequences that use a similar minimum number of transients to complete the cycle. For example, with the 5-step FSW sequence mentioned above, $\Delta\theta$ is roughly the same as that produced with depth pulse sequence (H) in Ref. 11 which requires a minimum of 24 transients to be collected, as opposed to the 27 transients required by FSW. In addition, at the expense of reduced SNR, high-flux signals from regions where $\theta = 270°$ can be eliminated in the FSW experiment using incremented flip angles in the VOI given by $n\theta = 60°$, 120°, 240°, etc. Likewise, both 270° and 450° high-flux regions can be suppressed using incremented flip angles in the VOI given by $n\theta = 45°$, 90°, 135°, 225°, 270°, etc.

Of note, when acquiring multivoxel data with phase-modulated RFZ, the Fourier series approach can be used to improve SNR by varying the number of transients averaged for each n, rather than multiplying by a weighting function during data processing.

A brief description of FSW theory is provided to facilitate an understanding of the method. For simplicity, relaxation and the undesirable consequences of applying pulses off-resonance are ignored. That is, if the RF pulse frequency can be assumed to be equal to the Larmor frequency Ω_2, then the signal equation can be written simply as

$$s(n, \Omega_2) = \int M_0(\mathbf{r}) \sin(\omega_1(\mathbf{r}) n t_p) \mathrm{d}\mathbf{r} \tag{4}$$

where $\omega_1(\mathbf{r})$ is the spatially dependent nutation frequency $(=\gamma B_1^{+}(\mathbf{r}))$ and $M_0(\mathbf{r})$ represents the longitudinal magnetization immediately before the $n\theta$ pulse. For simplicity, this signal equation incorporates experimental constants in M_0, including $B_1^{-}(\mathbf{r})$ and the receiver gain.

The general equation for a sine Fourier series is

$$W(\mathbf{r}) = \sum_{n=1}^{N} b_n \sin(\omega_1(\mathbf{r}) n t_p) \tag{5}$$

where b_n are the Fourier series coefficients and $W(\mathbf{r})$ is the desired window function that will be shown to define the range of $\theta(\mathbf{r})$ values in the localized region (the 'window'). The coefficients are given by

$$b_n = \frac{1}{n}[\cos(n\theta_a) - \cos(n\theta_b)] \tag{6}$$

where the borders of the window are described in terms of flip angles, θ_a and θ_b, which equal $\gamma B_1^{+}(\mathbf{r}_a)t_p$ and $\gamma B_1^{+}(\mathbf{r}_b)t_p$, respectively. By exploiting the trigonometric identity,

$$\cos(x) - \cos(y) = -2\sin((x+y)/2)\sin((x-y)/2) \tag{7}$$

equation (6) can be written as

$$b_n = \frac{2}{n}\sin(n\theta_k)\sin(n\delta) \tag{8}$$

Table 2. Fourier coefficients for constructing $\theta = 45^\circ, 60^\circ, 90^\circ, 120^\circ, 135^\circ$ windows in the phase-modulated FSW experiment

	Fourier coefficients a_n; b_n									
n	45°		60°		90°		120°		135°	
0	0.141;	0	0.141;	0	0.141;	0	0.141;	0	0.141;	0
1	0.197;	0.197	0.139;	0.241	0;	0.278	−0.139;	0.241	−0.197;	0.197
2	0;	0.269	−0.135;	0.233	−0.269;	0	−0.135;	−0.233	0;	−0.269
3	−0.179;	0.179	−0.254;	0	0;	−0.253	0.254;	0	0.179;	0.179
4	−0.233;	0	−0.117;	−0.202	−0.233;	0	−0.177;	0.202	−0.233;	0
5	−0.147;	−0.147	0.104;	−0.180	0;	0.208	−0.104;	−0.180	0.147;	−0.147
6	0;	−0.179	0.179;	0	−0.179;	0	0.179;	0	0;	0.179
7	0.105;	−0.105	0.074;	0.129	0;	−0.148	−0.074;	0.129	−0.105;	−0.105
8	0.116;	0	−0.058;	0.101	0.116;	0	−0.058;	−0.101	0.116;	0
9	0.060;	0.060	−0.085;	0	0;	0.084	0.085;	0	−0.060;	0.060
10	0;	0.054	−0.027;	−0.047	−0.054;	0	−0.027;	0.047	0;	−0.054
11	−0.018;	0.018	0.013;	−0.022	0;	−0.025	−0.013;	−0.022	0.018;	0.018

where $\theta_k = (\theta_a + \theta_b)/2$ and $\delta = (\theta_b - \theta_a)/2$. Substituting equation (8) into equation (5) yields

$$W(\theta_\mathrm{b} - \theta_\mathrm{a}) = \sum_{n=1}^{N} \frac{2}{n} \sin(n\theta_k)\sin(n\delta)\sin(n\theta) \tag{9}$$

It has been shown that Gibbs wobbles in this window function are minimized when $\delta = \pi/N$.[26] By combining equations (4) and (9), the expression describing the result of summing N FIDs weighted by Fourier coefficients is

$$\sum_{n=1}^{N} b_n s(n, \ \Omega_2) = \int M_0(\mathbf{r}) \sum_{n=1}^{N} b_n \sin(\omega_1 n t_\mathrm{p}) \mathrm{d}\mathbf{r}$$
$$= \int M_0(\mathbf{r}) W(\mathbf{r}_b - \mathbf{r}_\mathrm{a}) \mathrm{d}\mathbf{r} \tag{10}$$

When the Fourier coefficients are used to determine the number of transients to be averaged at each setting of n, the summation of equation (10) combines the signal and noise in the transients in an optimal manner (i.e., with equal weightings).

In phase-modulated RFZ, the cosine Fourier coefficients must also be used,[27] as given by

$$a_0 = \delta \tag{11a}$$

$$a_n = \frac{2}{n}\cos(n\theta_k)\sin(n\delta) \quad \text{for } n > 0 \tag{11b}$$

The window centered at phase increment $\theta_\mathrm{k}(\mathbf{r})$ is given by

$$W(\theta - \theta_k) = \sum_{n=0}^{N} \{a_n^k \cos(n\theta) + b_n^k \sin(n\theta)\} \tag{12}$$

where a_n^k and b_n^k are real numbers (the cosine and sine Fourier coefficients, respectively), and $b_0^k = 0$. Letting s_+ and s_- represent the signal following the $90^\circ[+y]$ and $90^\circ[-y]$ pulses, respectively, the signal equations are

$$s_+(n, \Omega_2) = \int M_0(\mathbf{r}) e^{i(\omega_1 n t_\mathrm{p} + \pi/2)} \mathrm{d}\mathbf{r} \tag{13}$$

and

$$s_-(n, \Omega_2) = \int M_0(\mathbf{r}) e^{-i(\omega_1 n t_\mathrm{p} + \pi/2)} \mathrm{d}\mathbf{r} \tag{14}$$

Adding equations (13) and (14) yields

$$\mathrm{SUM}(n, \Omega_2) = 2\int M_0(\mathbf{r}) \cos(\omega_1(\mathbf{r}) n t_\mathrm{p} + \pi/2)\, \mathrm{d}\mathbf{r} \tag{15}$$

whereas subtracting equations (13) and (14) yields

$$\mathrm{DIFF}(n, \Omega_2) = 2i\int M_0(\mathbf{r}) \sin(\omega_1(\mathbf{r}) n t_\mathrm{p} + \pi/2)\, \mathrm{d}\mathbf{r} \tag{16}$$

The signal localized in the window positioned at phase increment $\theta_\mathrm{k}(\mathbf{r})$ is then constructed according to

$$\sum_{n=0}^{N} \{a_n^\mathrm{k} \mathrm{DIFF}(n, \Omega_2) - i b_n^\mathrm{k} \mathrm{SUM}(n, \Omega_2)\}$$
$$= 2\int M_0(\mathbf{r}) \{a_n^\mathrm{k} \cos(\omega_1(\mathbf{r}) n t_\mathrm{p}) + b_n^\mathrm{k} \sin(\omega_1(\mathbf{r}) n t_\mathrm{p})\} \mathrm{d}\mathbf{r}$$
$$= 2\int M_0(\mathbf{r}) W(\theta - \theta_\mathrm{k}) \mathrm{d}\mathbf{r} \tag{17}$$

Tables 2 and 3 list Fourier coefficients and corresponding numbers of transients previously used in phase-modulated RFZ. One advantage of RFZ is the ability to shift the voxel locations after data have been acquired by postprocessing using different coefficients.[28]

Practical Implementations

Experimental Determination of Flip Angles

With conventional pulses, the amount of RF power needed to produce the correct flip angle in the VOI is dependent not only on its depth but also on the positioning of the object relative to the coil and its resistive load. Therefore, the setup procedures for a B_1-localized MRS measurement will usually require an empirical determination of $B_1{}^+(\mathbf{r})$. One experimental procedure preferred by this author is described here, but others may also suffice.

With a volume coil that produces a relatively uniform $B_1{}^+$, the power needed to achieve a 90° flip angle can be

Table 3. Number of acquisitions $N(n)$ and multiplication factors for phase-modulated FSW localization at $\theta = 45°$, $60°$, $90°$, $120°$, and $135°$

		Multiplication factors, c(a_n); c(b_n)									
n	$N(n)$	45°		60°		90°		120°		135°	
0	8	1.175;	0	1.175;	0	1.175;	0	1.175;	0	1.175;	0
1	20	0.675;	0.675	0.463;	0.803	0;	0.927	−0.463;	0.803	−0.657;	0.657
2	20	0;	0.897	−0.450;	0.777	−0.897;	0	−0.450;	−0.777	0;	−0.897
3	16	−0.746;	0.746	−1.058;	0	0;	−1.054	1.058;	0	0.746;	0.746
4	16	−0.971;	0	−0.488;	−0.842	0.971;	0	−0.488;	0.842	−0.971;	0
5	12	−0.817;	−0.817	0.578;	−1.000	0;	1.156	−0.578;	−1.000	0.817;	−0.817
6	12	0;	−0.994	0.994;	0	−0.994;	0	0.994;	0	0;	0.994
7	8	0.875;	−0.875	0.617;	1.075	0;	−1.233	−0.617;	1.075	−0.875;	−0.875
8	8	0.967;	0	−0.483;	0.842	0.967;	0	−0.483;	−0.842	0.967;	0
9	4	1.000;	1.000	−1.417;	0	0;	1.400	1.417;	0	−1.000;	1.000
10	4	0;	0.900	−0.450;	−0.783	−0.900;	0	−0.450;	0.783	0;	−0.900
11	4	−0.300;	0.300	0.217;	−0.367	0;	−0.417	−0.217;	−0.367	0.300;	0.300

determined in a series of simple experiments in which the pulse duration (or amplitude) is gradually increased until the on-resonance signal is maximized ($\theta = 90°$) or nulled ($\theta = 180°$). In this measurement, the TR should be sufficiently larger than T_1 (e.g., $>4T_1$) to avoid saturation effects. In addition, the carrier frequency should be placed directly on the spectral peak being used for calibration ($\Delta\nu = 0$). However, with a coil that produces a nonuniform $B_1{}^+$, this simple experiment will not suffice. In addition, in tissues the signal intensities of ^{31}P, ^{13}C, and other low-γ nuclei are usually too weak to permit rapid and accurate power calibrations by any means. Thus, as an alternative, a capillary vial filled with a ^{31}P or ^{13}C reference solution can be placed within the sensitive volume of the coil. To save time, the reference solution should provide signals strong enough to allow RF power calibration using minimal signal averaging, and the chemical shift should not overlap in vivo resonances. The calibration should be performed with the reference solution placed at a known location $\mathbf{r_0}$ relative to the coil (e.g., at the center of the surface coil). Then an electromagnetic field simulation or experimentally measured map of $B_1{}^+(\mathbf{r})$ is used to approximate the flip angle at any other location $\mathbf{r}$ using the relationship: $\theta(\mathbf{r}) = \theta(\mathbf{r_0}) \times B_1{}^+(\mathbf{r})/B_1{}^+(\mathbf{r_0})$. With depth pulse sequences, the duration of the excitation pulse should be adjusted to produce a 90° flip angle in the center of the VOI. To avoid aliasing in RFZ, the pulse increment must be chosen so that $\theta(\mathbf{r}) \leq 180°$ at any signal-generating location in the object.

Voxel Prescription

As discussed above, controlling the voxel shape with B_1 gradients can be challenging. VOI prescription with any localization technique requires precise knowledge of the field gradient(s) used to spatially encode the signals. Unlike the fields produced by B_0-gradient coils that are approximately linear functions of x, y, and z, the spatial profile of the surface coil produced $B_1{}^+(\mathbf{r})$ is much more complex, and consequently, the VOIs produced with B_1 gradients do not have rectilinear edges. In addition, because its geometry is complex and varies with position, the VOI cannot be specified using only three orthogonal dimensions (x, y, z) as done with B_0-gradient methods. One way to visualize the VOI is to calculate or experimentally measure the $\theta(\mathbf{r})$ map produced by the RF coil(s). Then, the degree of localization achieved for a given VOI location can be calculated using the equation that describes the spatial dependence of the signal produced by the particular sequence used. For example, when using the phase-modulated FSW-RFZ method, equation (12) can be used to calculate the relative signal amplitude in three-dimensional (3-D) space, provided that the calibration steps described above have been performed to estimate the reference flip angle map. The voxel geometries produced with the depth pulse sequence can likewise be calculated. The equations describing how the signal amplitude varies as a function of $\theta(\mathbf{r})$ for different depth pulse sequences can be found in the cited literature. Finally, slight differences in coil sizes and shapes are factors to consider when comparing data obtained in different laboratories.

Combining B_1- and B_0-gradient Methods

With all B_1-localization methods, two or more RF coils capable of generating different $B_1{}^+(\mathbf{r})$ distributions must be used to define the VOI with suitable precision. As described above, when using surface coils, the VOI can be placed at increasing depths along the spatial coordinate corresponding to the coil axis, but at positions increasingly lateral to the coil axis, the B_1 contours curve toward shallower depths; thus, the VOI is crescent shaped, which is less than ideal for many applications. For studies that require one or more well-defined VOIs positioned on or near the coil axis, the lateral dimensions of the VOI can be truncated by applying one or more additional pulses in the presence of a B_0 gradient. When implemented with actively shielded B_0 gradients or in a manner that is not sensitive to eddy currents, hybrid sequences that exploit both B_1 and B_0 gradients can provide robust, flexible, and optimal performance in some cases. A particularly successful implementation involves combining depth pulse, RFZ, or FSW with a 2-D version of the B_0-gradient method known as *image-selected in vivo spectroscopy* (*ISIS*; see ***Single-Voxel MR Spectroscopy***).[29] In 2-D ISIS, two spatially selective inversion pulses are applied in a prescribed way (using different on/off combinations, together with

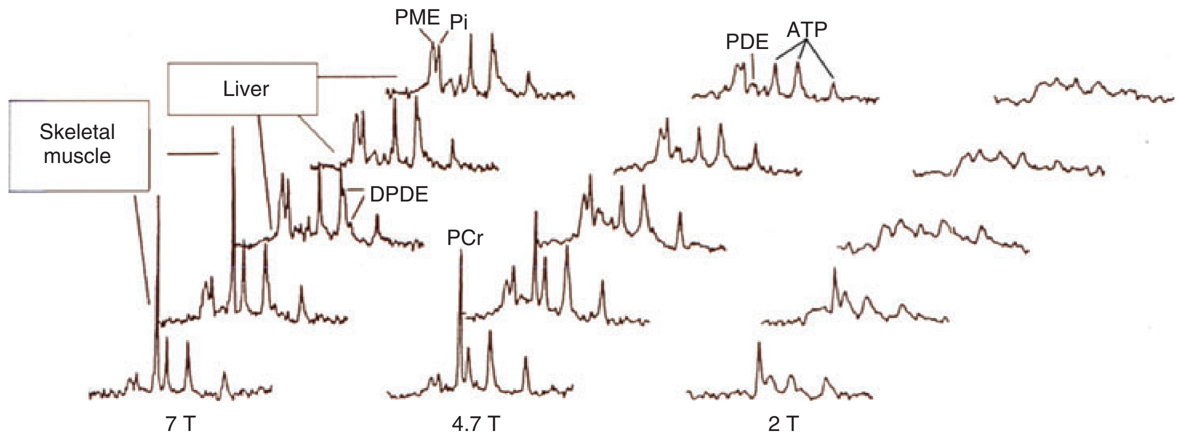

Figure 5. Examples of in vivo ^{31}P spectra that can be produced with a hybrid sequence based on FSW-RFZ and 2-D ISIS. These data sets were acquired from a single anesthetized rat using field strengths of 7, 4.7, and 2 T. The animal studies and care were approved by the University of Minnesota's Institutional Animal Care and Use Committee. Experiments were performed by transmitting and receiving with a single surface coil (diameter = 29 mm). To allow empirical estimation of the RF power settings to place the VOIs at the desired depths, each coil assembly included a small reference capillary containing 20 μl of 3 M phosphonoacetic acid at the coil center. The rat was placed prone with its liver centered over the capillary and coil. Signal acquisition was triggered by a controlled respiratory cycle (800 ms) to minimize motion artifact and to assure the anatomic region sampled was constant. A 12-term FSW was used. A single set of 1056 data acquisitions was processed to yield 5 voxels at increasing distances along the coil axis. Improved SNR and spectral resolution can be seen with increasing B_0. The deepest 2 voxels represent signal primarily from liver, as determined by the absence of PCr (PME = phosphomonoesters; PDE = phosphodiesters; DPDE = diphosphodiesters)

FID addition/subtraction) to localize signal to a column parallel to the surface coil axis.[22,27,30,31] Then, the third dimension (in the direction of the coil axis) can be localized using depth pulse, FSW, or RFZ methods. Exemplary ^{31}P spectra that were acquired with the latter approach are shown in Figure 5.

Discussion

This article has focused on just two B_1-localization methods, depth pulse and RFZ, as they are the ones most commonly used for in vivo MRS and ample evidence exists in literature showing the high spectral quality they are capable of producing. For brevity, descriptions of many variants of these, as well as several hybrid sequences using both B_1 and B_0 gradients, were not discussed in detail. Furthermore, although rotating frame methods for accomplishing slice-selective excitation exist, these were also not discussed as the methods developed so far have limitations (e.g., high RF power deposition) or have not been used for in vivo MRS.[10,32−36] This article also does not cover the rich body of work on performing homonuclear and heteronuclear spectral editing experiments with depth pulse[37−43] or RFZ[44] methods.

More than three decades have passed since these classic B_1-localization techniques were first introduced, and except for sporadic reports in the literature, developments in the past two decades have been modest at best. Following the development of actively shielded B_0-gradient coils, these techniques were largely superseded by B_0-gradient methods that offer greatly improved flexibility in controlling the dimensions and placement of VOI(s). Recently, however, interesting new approaches for performing MRI with B_1 gradients have appeared in the literature. These techniques are based on parallel imaging (PI) strategies that are now commonly used to accelerate image acquisition in MRI (e.g., SENSE[45]). Unlike PI techniques that use the receiver coils' sensitivity profiles ($B_1^-(\mathbf{r})$) for spatial encoding, these new B_1-gradient techniques exploit the amplitude and phase produced by the transmitted B_1^+ of a rotating surface coil[46] or utilize multiple spin echoes transmitted through B_1-gradient coils.[47] Other recent novel approaches have explored rotary-echo, echo-planar imaging (EPI) zeugmatography[48] and parallel transmit systems.[49] So far, investigations with these techniques have been confined to MRI applications, but future development will likely lead to single- and multivoxel MRS capabilities. The author believes that some version of these or a future new B_1-gradient technique could someday supersede or incorporate RFZ, FSW, and depth pulse methods, in conjunction with the now-popular B_0-gradient methods, to once again make B_1 localization a preferred approach to in vivo MRS. Only time will tell.

Acknowledgments

The author is grateful for support provided by NIH grants R24MH105998 and P41EB015894 and the Malcolm B. Hanson Professorship in Radiology. The author is indebted to colleagues who helped obtain the data shown in Figure 5; namely, Dr. Hellmut Merkle who built the surface coils, Dr. Sally Weisdorf who anesthetized and monitored the animals during data acquisitions, and Ms. Kristy Hendrich who acquired the 4.7 T ^{31}P data.

Biographical Sketch

Michael Garwood. b. 1957. BA, 1981, PhD, 1985, University of California, Santa Cruz. As a graduate student in chemistry, he developed pulse sequences for spatially localized spectroscopy. He moved to the University of Minnesota in 1986, where he designed new types of frequency-modulated pulses including low-angle adiabatic pulses and applied these and other advanced techniques in studies of cancer, neurodegeneration, and other diseases. He holds the Malcolm B. Hanson Professorship of Radiology and is an Associate Director of the Center for Magnetic Resonance Research at the University of Minnesota. In 2007, he was awarded the Gold Medal of the International Society of Magnetic Resonance in Medicine for his contributions to the field. His research interests include novel radiofrequency pulse design and applications of in vivo magnetic resonance spectroscopy and imaging.

References

1. J. J. Ackerman, T. H. Grove, G. G. Wong, D. G. Gadian, and G. K. Radda, *Nature*, 1980, **283**, 167.
2. P. A. Bottomley, T. B. Foster, and R. D. Darrow, *J. Magn. Reson.*, 1969, 1984, **59**, 338.
3. S. Müller, W. P. Aue, and J. Seelig, *J. Magn. Reson.*, 1969, 1985, **63**, 530.
4. R. Tycko and A. Pines, *J. Magn. Reson.*, 1969, 1984, **60**, 156.
5. A. J. Shaka and R. Freeman, *J. Magn. Reson.*, 1969, 1984, **59**, 169.
6. A. J. Shaka and R. Freeman, *J. Magn. Reson.*, 1969, 1985, **63**, 596.
7. A. J. Shaka and R. Freeman, *J. Magn. Reson.*, 1969, 1985, **62**, 340.
8. G. Bodenhausen, R. Freeman, and D. L. Turner, *J. Magn. Reson.*, 1969, 1977, **27**, 511.
9. M. R. Bendall and R. E. Gordon, *J. Magn. Reson.*, 1969, 1983, **53**, 365.
10. D. I. Hoult, *J. Magn. Reson.*, 1969, 1979, **33**, 183.
11. M. R. Bendall and D. T. Pegg, *Magn. Reson. Med.*, 1985, **2**, 91.
12. M. R. Bendall, *J. Magn. Reson.*, 1969, 1984, **59**, 406.
13. A. J. Shaka and R. Freeman, *J. Magn. Reson.*, 1969, 1985, **64**, 145.
14. M. R. Bendall and D. T. Pegg, *J. Magn. Reson.*, 1969, 1986, **68**, 252.
15. M. R. Bendall, D. Foxall, B. G. Nichols, and J. R. Schmidt, *J. Magn. Reson.*, 1969, 1986, **70**, 181.
16. S. J. Cox and P. Styles, *J. Magn. Reson.*, 1969, 1980, **40**, 209.
17. A. Haase, C. Malloy, and G. K. Radda, *J. Magn. Reson.*, 1969, 1983, **55**, 164.
18. M. Garwood, T. Schleich, G. B. Matson, and G. Acosta, *J. Magn. Reson.*, 1969, 1984, **60**, 268.
19. P. Styles, C. A. Scott, and G. K. Radda, *Magn. Reson. Med.*, 1985, **2**, 402.
20. M. Garwood and Y. Ke, *J. Magn. Reson.*, 1969, 1991, **94**, 511.
21. M. Garwood, P.-M. Robitaille, and K. Uğurbil, *J. Magn. Reson.*, 1969, 1987, **75**, 244.
22. P. M. Robitaille, H. Merkle, E. Sublett, K. Hendrich, B. Lew, G. Path, A. H. From, R. J. Bache, M. Garwood, and K. Ugurbil, *Magn. Reson. Med.*, 1989, **10**, 14.
23. J. Pekar, J. S. Leigh Jr, and B. Chance, *J. Magn. Reson.*, 1969, 1985, **64**, 115.
24. K. R. Metz and R. W. Briggs, *J. Magn. Reson.*, 1969, 1985, **64**, 172.
25. M. Garwood, T. Schleich, B. D. Ross, G. B. Matson, and W. D. Winters, *J. Magn. Reson.*, 1969, 1985, **65**, 239.
26. M. Garwood, T. Schleich, M. R. Bendall, and D. T. Pegg, *J. Magn. Reson.*, 1969, 1985, **65**, 510.
27. K. Hendrich, H. Merkle, S. Weisdorf, W. Vine, M. Garwood, and K. Uğurbil, *J. Magn. Reson.*, 1969, 1991, **92**, 258.
28. K. Hendrich, H. Liu, H. Merkle, J. Zhang, and K. Uğurbil, *J. Magn. Reson.*, 1969, 1992, **97**, 486.
29. R. J. Ordidge, A. Connelly, and J. A. B. Lohman, *J. Magn. Reson.*, 1986, **66**, 283.
30. J. W. Pan, H. P. Hetherington, J. R. Hamm, D. L. Rothman, and R. G. Shulman, *J. Magn. Reson.*, 1969, 1989, **81**, 608.
31. P. M. Robitaille, H. Merkle, B. Lew, G. Path, K. Hendrich, P. Lindstrom, A. H. L. From, M. Garwood, R. J. Bache, and K. Uğurbil, *Magn. Reson. Med.*, 1990, **16**, 91.
32. D. I. Hoult, *J. Magn. Reson.*, 1969, 1980, **38**, 369.
33. L. K. Hedges and D. I. Hoult, *J. Magn. Reson.*, 1969, 1988, **79**, 391.
34. J. Kaczyński, N. J. F. Dodd, and B. Wood, *J. Magn. Reson.*, 1969, 1992, **100**, 453.
35. G. S. Karczmar, T. J. Lawry, M. W. Weiner, and G. B. Matson, *J. Magn. Reson.*, 1969, 1988, **76**, 41.
36. D. Canet, D. Boudot, A. Belmajdoub, A. Retournard, and J. Brondeau, *J. Magn. Reson.*, 1969, 1988, **79**, 168.
37. H. P. Hetherington, J. R. Hamm, J. W. Pan, D. L. Rothman, and R. G. Shulman, *J. Magn. Reson.*, 1969, 1989, **82**, 86.
38. C. C. Hanstock, M. R. Bendall, H. P. Hetherington, D. P. Boisvert, and P. S. Allen, *J. Magn. Reson.*, 1969, 1987, **71**, 349.
39. M. R. Bendall and D. T. Pegg, *J. Magn. Reson.*, 1969, 1984, **57**, 337.
40. D. T. Pegg and M. R. Bendall, *J. Magn. Reson.*, 1969, 1985, **63**, 556.
41. M. R. Bendall and D. T. Pegg, *Magn. Reson. Med.*, 1985, **2**, 298.
42. D. T. Pegg and M. R. Bendall, *Magn. Reson. Med.*, 1985, **2**, 453.
43. M. R. Bendall, J. A. D. Hollander, F. Arias-Mendoza, D. L. Rothman, K. L. Behar, and R. G. Shulman, *Magn. Reson. Med.*, 1985, **2**, 56.
44. F. Mitsumori and N. M. Bolas, *J. Magn. Reson.*, 1969, 1992, **97**, 282.
45. K. P. Pruessmann, M. Weiger, M. B. Scheidegger, and P. Boesiger, *Magn. Reson. Med.*, 1999, **42**, 952.
46. A. Trakic, J. Jin, E. Weber, and S. Crozier, *Comput. Math. Methods Med.*, 2014, **2014**, 11.
47. J. C. Sharp and S. B. King, *Magn. Reson. Med.*, 2010, **63**, 151.
48. F. Casanova, H. Robert, J. Perlo, and D. Pusiol, *J. Magn. Reson.*, 2003, **162**, 396.
49. U. Katscher, J. Lisinski, P. Boernert, and I. Graesslin, *Joint Annual Meeting ISMRM-ESMRMB*, 2007, p. 679.